Experimental and theoretical determination of the metastable Fe-V phase diagram

J. M. Sanchez
Center for Material Science and Engineering, The University of Texas at Austin, Austin, Texas 78712

M. C. Cadeville and V. Pierron-Bohnes
Institut de Physique et Chimie des Matériaux de Strasbourg, Groupe d'Etude des Matériaux Métalliques UMR 46 CNRS, Université Louis Pasteur, 23 rue du Loess, F-67037 Strasbourg, France

G. Inden
Max Planck Institute für Eisenforschung, Max-Planck Strasse 1, D-4000 Düsseldorf, Germany
(Received 29 May 1996)

The Fe-V phase diagram is calculated in the cube-rhombohedron-octahedron approximation of the cluster variation method for four sets of effective pair interactions that include up to fifth neighbors. Two of the sets of pair interactions were determined using a real space inverse cluster variation method from short-range order intensity data measured at 1133 and 1473 K in a Fe-19.6%V single crystal. The other two sets of interactions were previously calculated by Sluiter and Turchi in the Fe_3V and FeV systems using electronic structure methods. The results are compared to experimental data for the metastable phase diagram. The phase diagrams obtained from the short-range order intensity measurements are in good agreement with the experimental data. [S0163-1829(96)07238-4]

In this report we present experimental results for the low-temperature part of the metastable Fe-V phase diagram and compare these and other available data to the phase diagram calculated in the cube-rhombohedron-octahedron (CRO) approximation of the cluster variation method (CVM) using various sets of effective pair interactions (EPI). Two sets of experimental EPI's were deduced from short-range order (SRO) intensity measured at 1133 and 1473 K (Ref. 1) using a real space inverse CVM in the CRO cluster approximation. Two other sets of EPI's were those calculated by Sluiter and Turchi[2] using a simple electronic structure method based on a tight-binding approximation.

The assessed Fe-V phase diagram displays a continuous high-temperature bcc solid solution intersected at lower temperatures, below 1500 K, by a σ phase centered around equiatomic composition.[3] Due to the very sluggish character of the bcc to σ transformation it is possible to retain the bcc solid solution at low temperatures. This metastable solid solution has a tendency to order with a CsCl-type structure ($B2$).[4] Using differential thermal analysis, Seki *et al.*[4] have measured the critical order-disorder transformation temperature (T_c) as a function of concentration for ten alloys with atomic concentrations ranging between 30% and 70% V. Their results are displayed in Fig. 1. For V concentrations of 48%, 55%, 56.7%, and 61.4%, the values of T_c were extrapolated from the results of ternary alloys. The concentration dependence of T_c displays a nearly symmetric parabolic behavior, which would be expected from a simple model based on concentration-independent pair interactions. Here we focus our attention on the experimental determination of the low-temperature part of the phase diagram which until now was unknown.

A point of interest in the present study is to establish the nature of the $B2$ ordering transitions at low temperatures. Theoretical models suggest that the transitions between the disorder bcc ($A2$) and the ordered ($B2$) phases is second order around the one-to-one (AB) stoichiometry.[5] In the absence of second-neighbor interactions, the transition remains second order down to 0 K. With second-neighbor interactions present, a different phase diagram topology is observed around the three-to-one stoichiometry (A_3B). In this case,

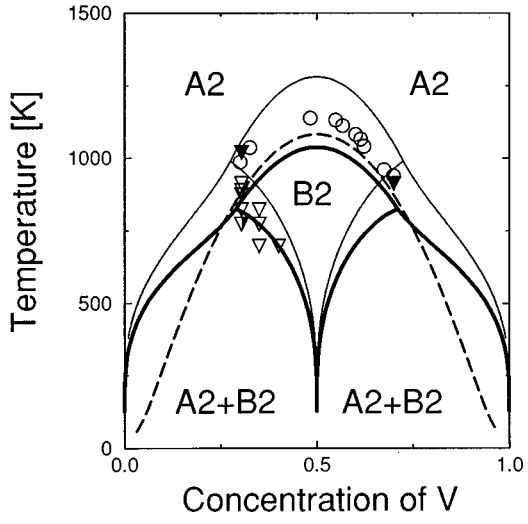

FIG. 1. The $B2$-$A2$ order-disorder transition temperatures from Ref. 4 (circles). The $B2$, $B2+A2$, and $A2$ phase regions determined from TEM observations are shown, respectively, by the full, half-full, and empty triangles. Thin and thick lines are the calculated phase diagram with experimental EPI's deduced in Ref. 1 from SRO measurements at, respectively, 1133 and 1473 K. The dashed line is the phase diagram calculated using the theoretical EPI's obtained in Ref. 2 with ODD effect. (The phase diagram calculated with EPI's without ODD, out of the scale of the figure, is not shown.)

the line of second order transitions either ends at a tricritical point, below which the transition becomes first order with the characteristic two-phase ($A2+B2$) region, or the $B2$ phase transforms to a $DO3$ ordered structure. Golosov and Tolstik[6] were among the first to calculate the bcc phase diagram in the tetrahedron approximation of the CVM including both nearest-neighbor (V_1) and next-nearest-neighbor (V_2) pair interactions. It is now well known that the resulting phase diagram yields a two-phase field $A2+B2$ at low temperature for V_1 attractive (>0) and V_2 repulsive (<0). When V_1 and V_2 are both attractive, i.e., in the frustrated regime, the $DO3$ phase appears for $V_2/V_1<2/3$.[6–9] This phase diagram topology is actually observed in the Fe-Al system for example.[8,10]

In order to determine the nature of the order-disorder transition in the Fe-V system, an electron microscopy study was performed for three samples with atomic concentrations of V of 30%, 35%, and 40% for various annealing temperatures and annealing times. The specimen were homogenized for three days in quartz capsules at 1403 K, a temperature that corresponds to the disordered bcc solid solution (Fig. 1), and subsequently water quenched. After this treatment, transmission electron microscopy (TEM) observations show weak $B2$ superlattice reflections, indicating that the ordering reaction could not be suppressed by quenching. This is a common observation related to the high concentration of thermal vacancies retained during quenching. If the quench temperature is below the ordering transition, the diffusion of vacancies associated with thermal equilibration produces ordering. Due to the high degree of supersaturation of thermal vacancies, this ordering process takes place rapidly throughout the sample leading to the formation of small antiphase domains (APD) and, thus, weak superlattice reflections. In the present case, the APD size was in the range of 0.05-0.1 μm, as observed in dark field using the [110] superlattice reflection. At an atomic concentration of 30% V, annealing at 823 K for 46 days resulted in considerable growth in the APD size, as shown in Fig. 2(a). It is noted that the same domain size was already achieved after an annealing time of 14 days. Tilting the specimen resulted in a contrast reversal that is characteristic of antiphase domain boundaries (APB). This contrast reversal can also be seen at the boundary of the reflection zone due to bending of the thin foils [see dark region at the top of Fig. 2(a)]. From these observations, it is concluded that the equilibrium state at 823 K is single phase $B2$. Similar observations were made at higher temperatures, establishing that $B2$ is the equilibrium phase in Fe-30%V up to 913 K. For the compositions 35% and 40% V, the $B2$ phase was determined to be the equilibrium phase down to 700 K (see Fig. 1).

After annealing the specimen with 30% V at 773 K for 17 days, it was found that the domain size was the same as observed immediately after the quench [see Fig. 2(b)]. Furthermore, tilting of the specimen did not produce contrast reversal. The same holds for the regions out of the reflection zone in Fig. 2(b). This suggests that the dark regions are disordered phase which cannot be brought into bright contrast with a $B2$-type reflection. Although the lack of contrast reversal may not be considered conclusive evidence of a disordered phase, together with the lack of domain growth after annealing is indicative of the presence of a two-phase mixture of ordered $B2$ and disordered $A2$ that formed at preexisting APB after quenching. It is noted that the same annealing treatment (773 K for 17 days) applied to the Fe-35%V sample leads to a microstructure very similar to that of Fig. 2(a), in which there has been considerable coarsening of the APD. This indicates that the lack of domain growth in the Fe-30%V shown in Fig. 2(b) cannot be attributed to low diffusivity. Finally, in the diffraction mode, no evidence was found for the presence of the DO_3 phase. In summary, the TEM observations strongly suggest that the Fe-V phase diagram displays a low-temperature $A2+B2$ two-phase field around an atomic composition of about 30% V.

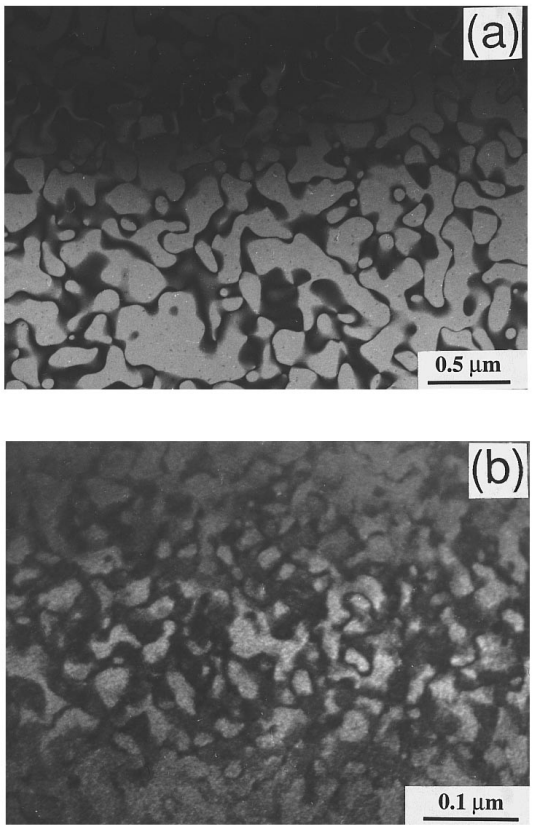

FIG. 2. Dark field TEM observations with the $B2$ superlattice reflection [100]. Samples were heat treated for 3 days at 1403 K followed by a quench and 46 days at 823 K (a), or for 17 days at 773 K (b).

In an attempt to reproduce this phase diagram, we used both experimental[1] and calculated[2] EPI's for the first five neighbor shells. The experimental interactions are those obtained from neutron SRO intensities as described in Ref. 1. These interaction were extracted from the data by modeling the measured SRO intensity with a simple Ising Hamiltonian in which the magnetic moments were assumed to be localized on the Fe atoms. In terms of interatomic potentials between different chemical species, the effective interactions are given by

$$V_{pp'}=\tfrac{1}{4}[V_{pp'}^{\mathrm{FeFe}}+V_{pp'}^{\mathrm{VV}}-2V_{pp'}^{\mathrm{FeV}}]. \tag{1}$$

These effective interactions include both effective chemical ($V_{pp'}^{\mathrm{C}}$) and exchange magnetic ($J_{pp'}$) interactions between sites R_p and $R_{p'}$, according to the expression:

TABLE I. Pair interactions (in meV) from Refs. 1 and 2.

Experimental EPI's in Fe-19.6%V		Calculated EPI's from Ref. 2		
n	$T=1133$ K	$T=1473$ K	Fe_3V (without ODD)	FeV (with ODD)
1	9.8 (0.4)	8.2 (0.6)	23.0	8.90
2	−1.2 (0.6)	−3.6 (0.7)	2.2	0.32
3	−4.6 (0.4)	−2.9 (0.5)	1.0	1.20
4	−1.2 (0.4)	−1.2 (0.4)	1.5	1.50
5	−1.9 (0.5)	−1.5 (0.5)	−3.2	−1.55

$$V_{pp'}=V^{C}_{pp'}-\tfrac{1}{4}J_{pp'}\langle S_pS_{p'}\rangle, \tag{2}$$

where S_p is the spin operator (± 1) at site R_p.

The Warren-Cowley SRO parameters deduced from the Fourier transform of the SRO intensity were fitted using the inverse cluster variation method (CVM) algorithm proposed by Gratias and Cénédèse.[11] The CVM approximation used in the inverse method includes three maximum clusters: the body-centered cube, the eight-point rhombohedron, and the octahedron, called here the CRO approximation. The approximation allows to determine the first five effective interactions in the bcc lattice. The EPI's obtained for the two measurement temperatures are given in Table I. There is a weak dependence of the ECI's with temperature, which is most likely due to changes in the magnetic SRO. The magnetic short-range order, $\langle S_pS_{p'}\rangle$, which is expected to become negligible in the limit of high-temperatures, is still important at 1133 K, a temperature that is close to the Curie temperature of the alloy ($T_c=1073$ K).

The theoretical sets of EPI's for the first five coordination shells were obtained by Sluiter and Turchi[2] using a simple tight-binding Hamiltonian treated in the coherent potential approximation (CPA). These authors carried out their calculations for three compositions: Fe_3V, FeV, and FeV_3. For Fe_3V and FeV_3, the Hamiltonian did not include off-diagonal disorder (ODD), whereas ODD was taken into account for FeV. Table I shows the sets of EPI's calculated for Fe_3V (without ODD) and FeV (with ODD). Note that the values in Table I are smaller by a factor of 4 relative to the values reported in Ref. 2, consistent with the different definition of EPI's used in Eq. (1). A striking difference between the interactions obtained with and without ODD is evident from the results of Table I.

The corresponding phase diagrams calculated in the CRO approximation of the CVM for the different sets of interactions are shown in Fig. 1. Note that the two-phase field $A2+B2$ observed at low temperatures is only reproduced using the set of experimental EPI's obtained from the SRO intensity measurements. We recall that the two phase field is expected to be present when the sign of V_1 and V_2 are different. This particular feature of the interactions is described well by the experimental EPI's, as suggested by the agreement between the calculated and the experimental phase diagram. In contrast, we note that the theoretical EPI's calculated by Sluiter and Turchi[2] fail to reproduce the correct sign of the second-neighbor interactions, thus leading to the wrong topology of the predicted phase diagram. The phase diagram corresponding to the EPI's obtained without ODD is not shown in Fig. 1 since the predicted phase boundaries come at a much higher temperature than observed experimentally. Thus, in the absence of ODD, the model significantly overestimates the values of the nearest-neighbor interaction V_1. We note that similar results for the EPI's are obtained from a more elaborate treatment of the electronic structure of Fe-V disordered alloys.[12] The nearest neighbor EPI's calculated including the effect of ODD are then in better agreement with experiment although, as mentioned, the predicted sign of the second-neighbor interactions is wrong.

To conclude, we have established the low-temperature topology of the metastable phase diagram in the Fe-V system. The experimental phase diagram determinations have been critically tested against several theoretical and semiempirical methods. Good agreement was found between the experimental phase diagram and that obtained with a high-level approximation of the CVM using the EPI's extracted from SRO intensity measurements. These results are particularly encouraging since the details of the phase diagram depend critically on the values of the EPI's. Finally, the experimental results show qualitative disagreement between the actual phase diagram and that predicted with the EPI's obtained by Sluiter and Turchi.[2]

The work at The University of Texas at Austin was supported by the National Science Foundation under Grants No. DMR-91-14646 and No. INT-91-14645.

[1] V. Pierron-Bohnes, E. Kentzinger, M.C. Cadeville, J.M. Sanchez, R. Caudron, F. Solal, and R. Kozubski, Phys. Rev. B **51**, 5760 (1995).

[2] M. Sluiter and P.E.A. Turchi, in *High-Temperature Ordered Intermetallic Alloys*, edited by L.A. Johnson, D.P. Pope, and J.O. Stiegler, MRS Symposia Proceedings No. 213 (Materials Research Society, Pittsburgh, 1991), p. 37.

[3] O. Kubaschewski, in *Iron-Binary Phase Diagrams* (Springer-Verlag, Berlin, 1982), pp. 160–164.

[4] J.I. Seki, M. Hagiwara, and T. Suzuki, J. Mater. Sci. **14**, 2404 (1979).

[5] F. Ducastelle, in *Order and Phase Stability in Alloys*, edited by

R.R. de Boer and D.G. Pettifor (North-Holland, Amsterdam, 1991).
[6] N.S. Golosov and A.M. Tolstik, J. Phys. Chem. Solids **36**, 899 (1975).
[7] D.A. Contreras-Solorio, F. Mejía-Lira, J.L. Morán-López, and J.M. Sanchez, Phys. Rev. B **38**, 4955 (1988).
[8] D.A. Contreras-Solorio, F. Mejía-Lira, J.L. Morán-López, and J.M. Sanchez, Phys. Rev. B **38**, 11 481 (1988).
[9] H. Ackermann, G. Inden, and R. Kikuchi, Acta Metall. **37**, 1 (1989).
[10] J.M. Sanchez, V. Pierron-Bohnes, and F. Mejía-Lira, Phys. Rev. B **51**, 3429 (1995).
[11] D. Gratias and P. Cénédèse, J. Phys. **46**, C9-149 (1985).
[12] P.E.A. Turchi, L. Reinhard, and G. M. Stocks, Phys. Rev. B **50**, 15 542 (1994).